REPORT DOCUMENTATION PAGE

Form Approved
OMB No. 0704-0188

1. AGENCY USE ONLY (Leave blank)	2. REPORT DATE	3. REPORT TYPE AND DATES COVERED
	February 16, 1996	Final Report

4. TITLE AND SUBTITLE
Mechanics of Smart Structures

5. FUNDING NUMBERS
F49620-92-J-0342

6. AUTHOR(S)
J. D. Achenbach
S. Krishnaswamy

7. PERFORMING ORGANIZATION NAME(S) AND ADDRESS(ES)
Northwestern University

8. PERFORMING ORGANIZATION REPORT NUMBER
AFOSR-TR-96
0283

9. SPONSORING/MONITORING AGENCY NAME(S) AND ADDRESS(ES)
Airforce Office of Scientific Research
Bolling AFB, Washington D.C.

NA

92-J-0342

11. SUPPLEMENTARY NOTES

12a. DISTRIBUTION/AVAILABILITY STATEMENT
Unrestricted

12b. DISTRIBUTION CODE

13. ABSTRACT (Maximum 200 words)
This work deals with the development of fiber-optic ultrasound sensors. A frequency-stabilized fiber-optic fabry-perot (FSI-FOFP) sensor has been devised. The sensor has been used to detect pzt and laser-generated ultrasound. Applications to flaw detection have been demonstrated. Theoretical calculations have been performed to obtain the frequency response of the FSI-FOFP embedded in expoxy, and the calculations have been verified experimentally.

19960617 128

14. SUBJECT TERMS
Fiber Optic Ultrasound Sensors

15. NUMBER OF PAGES
19

16. PRICE CODE

17. SECURITY CLASSIFICATION OF REPORT	18. SECURITY CLASSIFICATION OF THIS PAGE	19. SECURITY CLASSIFICATION OF ABSTRACT	20. LIMITATION OF ABSTRACT
Unclassified	Unclassified	Unclassified	U

Mechanics of Smart Structures

Final Project Report
submitted to the

Air Force Office of Scientific Research
Aerospace Sciences Directorate

Submitted by

Sridhar Krishnaswamy
(708) 491-4006

Jan D. Achenbach
(708) 491-5527

February 16, 1996

CENTER FOR QUALITY ENGINEERING AND FAILURE PREVENTION
NORTHWESTERN UNIVERSITY
Evanston, Illinois 60208-3020

TABLE OF CONTENTS

MECHANICS OF SMART STRUCTURES:

EXECUTIVE SUMMARY

A new concept to monitor structural health utilizes a network of sensors which are integrated into a structure during fabrication or retrofitted to existing structures. Information from the sensor network can be used in conjunction with a system of actuators to alter geometrical or vibrational characteristics of the structure enabling continued safe operation. Such structures have been termed 'smart structures'.

In the most general scheme, the network of sensors can be used throughout the entire design life of the structure. Initially, during fabrication the sensor network can provide information to monitor and control processing. Such a scheme could eliminate the need for post processing inspection by actively controlling the manufacturing process and informing an operator if a part is defective. During service, the same network of sensors can be used to monitor structural integrity and provide information to actuators which control structural characteristics. Such a scheme would offer a dramatic savings in the time and cost associated with taking a structure out of service and inspecting it. The inspection of a 'smart structure' could be performed during service. Finally, sensors can provide information during the onset of structural failure and give warning when the actuators can no longer take corrective action. The work completed at Northwestern University has concentrated on the development of fiber-optic ultrasonic sensors to detect and characterize critical flaws in aircraft structures.

In this work some of the issues which have hindered fiber optic ultrasound sensors from becoming a viable 'smart structure' sensing technology have been addressed. A technique has been developed to stabilize a localized fiber optic Fabry-Perot interferometer at its most sensitive operating point, namely quadrature. Maintaining quadrature is essential when detecting the very small displacements associated with ultrasound. Stabilization is accomplished by actively tuning the laser frequency to compensate for mechanical and thermal drifts and maintain quadrature. The utility of this scheme is demonstrated by detecting ultrasound with a stabilized and unstabilized interferometer in the presence of mechanical stressing.

An optical technique for the generation of ultrasound using fiber optics has also been developed. The approach uses a high power pulsed laser and a high power optical fiber to generate ultrasound. Two different generation schemes have been investigated. The first technique generates ultrasound at a given point inside a structure by embedding the delivery fiber into the host material. The second technique uses a light pulse which

exits the optical fiber and generates ultrasound at a prepared location on the surface. Both techniques offer the potential to generate ultrasound in the presence of electromagnetic interference and at elevated temperatures.

A theoretical model was also developed which predicts the response of an embedded fiber optic ultrasound sensor for a given host material. This is essential because of the wide range of host materials into which a fiber optic ultrasound sensor can be embedded. Calculations were performed for a fiber sensor embedded in epoxy subjected to a normally incident harmonic plane wave. The frequency of the incident wave was then changed to investigate the fiber response as a function of frequency. The calculated results for a fiber in epoxy were verified experimentally, and the details of the experimental approach are described.

List of personnel: John Dorighi, Sridhar Krishnaswamy, Jan Achenbach

List of publications stemming from research effort:

Dorighi, J.F., Sridhar Krishnaswamy and Jan D. Achenbach, "Stabilization of an Embedded Fiber Optic Fabry-Perot Sensor for Ultrasound Detection," IEEE Transactions on Ultrasonics, Ferroelectrics and Frequency Control, vol .42, No. 5, pp. 820-824, 1995.

Dorighi, J.F., Sridhar Krishnaswamy and Jan D. Achenbach, "Fiber-Optic Laser Generation and Detection of Ultrasound", SPIE Proceedings, vol. 2574, pp.46-53, 1995.

Dorighi, J.F., Sridhar Krishnaswamy and Jan D. Achenbach, "Laser-based Ultrasonics using Fiber-Optic Laser Generation and Detection of Ultrasound", SPIE Proceedings, vol. 2622, pp. 274-278, 1995.

Dorighi, J.F., Sridhar Krishnaswamy and Jan D. Achenbach, "Embedded Fiber-Optic Fabry-Perot Sensors for Ultrasound Detection," in Rev. Progress in QNDE, ed. D.O. Thompson and D.E. Chimenti, vol. 14, Plenum Press, New York.

Dorighi, J.F., Sridhar Krishnaswamy and Jan D. Achenbach, "Stabilization of an Embedded Fiber-Optic Ultrasound Sensor for Cure Monitoring of an Epoxy Plate," in Rev. Progress in QNDE, ed. D.O. Thompson and D.E. Chimenti, vol. 15, Plenum Press, New York.

Dorighi, J.F., Sridhar Krishnaswamy and Jan D. Achenbach, "Frequency Response of Fiber Optic Ultrasound Sensors," to appear Proc. IEEE UFFC Symposium, Seattle, Nov. 7-10, 1995.

Dorighi, J.F., (1994), M.S. Dissertation, Northwestern University.

I. Introduction

The objective of this work was to develop fiber-optic ultrasonic sensors for the detection and characterization of critical flaws in aircraft structures as part of a timely quantitative nondestructive evaluation (QNDE) program. QNDE is an interdisciplinary process encompassing quantitative measurement techniques to identify and characterize flaws, coupled with measurement models to interpret and relate the data to considerations of structural integrity and remaining life time of a component. The complete QNDE process therefore requires drawing on the resources of sensor technology, fracture mechanics and materials science to obtain reliable estimates of remaining safe life for a structure given the flaw characteristics as measured by a reliable NDE tool.

The Air Force fleet must operate under diverse and often severe environmental conditions, and the methods of QNDE will play an increasing role in the in-service monitoring and maintenance of the currently aging fleet as well as of future structural systems incorporating advanced composite materials and metals. Flaw sites which are introduced into structural components during materials processing can be the source of fatigue cracking and corrosion damage which can severely compromise the structural integrity and effective performance of Air Force systems. Many critical areas of aircraft structures such as the interiors of fuel tanks and interfaces in multi-layered components are not readily accessible for inspection using conventional NDE techniques. Improved methods for the timely detection and characterization of flaws are therefore needed to assess the safety of aircraft structures. This project has addressed the development of an important NDE tool utilizing fiber-optic ultrasonic sensors which can be permanently mounted in inaccessible regions of an airframe so as to facilitate flaw detection and characterization. The related structural reliability issues will not be specifically addressed here but other ongoing projects at our Center deal with those aspects.

1.1 Active Aerospace Structures: The ultimate goal of this project was to further the development of the concept of "active" structures. Active structures are structures that have an integrated array of sensors that can serve as a nervous system for structural health monitoring. These sensors are implanted in the material during composite materials processing (or retrofitted externally on metal structures) and can subsequently be used for continuous monitoring of the mechanical and material integrity of the structural components. This approach is expected to lead to better quality control of fabrication processes of composite materials, facilitate maintenance by providing continuous nondestructive evaluation of critical airframe structures, and can even be used

in conjunction with embedded actuators to alter the geometric and vibrational characteristics of a structure. The active structures concept is finding increasingly wide application in areas ranging from advanced aerospace structures and adaptive optics (telescope mirrors etc), to more mundane structures such as bridges and high-rise buildings [Udd (1995)].

1.2 Fiber-Optic Ultrasound Sensors: Fiber-optic sensors, in particular, are beginning to play a significant role in QNDE of active or smart structures in view of their (i) relatively high sensitivity to temperature and strain variations; (ii) ease of multiplexing of several sensors thereby bringing unit cost down; (iii) potential for use near inflammable chemicals (e.g. fuel) where conventional electrical sensors might pose a fire hazard; and above all (iv) their ability to survive and perform in very adverse environments including high temperatures and electromagnetic interference [Udd (1995), Udd (1991), Grattan & Meggitt (1995)]. While most fiber-optic sensors for smart structures applications have targeted low-frequency strain and temperature measurement [Udd (1995)], or rely on fiber-breakage to indicate the presence of a flaw [Measures (1991)], our approach at Northwestern University has been to use *ultrasonic* probe signals for defect detection, and to use optical systems both for the generation and detection of the ultrasound probe signal. The main advantage of this approach is that it is a truly active integrated nondestructive system which makes use of the above-mentioned advantages of optical systems, but couples them with ultrasonic probe signals which have a higher sensitivity for detecting localized damaged regions than any of the currently used purely optical embedded NDE systems [Claus and Thompson (1991)]. Note also that this approach does not require that the flaw be in the immediate vicinity of the fiber sensor for it to be detected since the generated ultrasonic waves can be suitably directed to probe different regions of the structure. Another attractive feature of fiber-optic sensors is that they are very broadband detectors with frequency response well into the ultrasonic range, which makes them highly suitable for broadband acoustic and ultrasonic detection [Dorighi, Krishnaswamy & Achenbach (1995a)]. The detection can be passive to monitor acoustic emission signals and the vibrational modes of structures. Alternatively, in conjunction with pzt- or laser-generation of ultrasound these sensors can be used to actively probe the structure for incipient critical flaws.

1.3 Outline of Work Completed at Northwestern University: The major aspects involved in fiber-optic ultrasonic sensor development include: sensor development; sensor characterization and associated signal-to-noise considerations; and sensor multiplexing

and associated data transfer issues. At the Center for Quality Engineering at Northwestern University, we have been involved in the development of intrinsic fiber-optic systems for laser generation and detection of ultrasound inside a structure. We have successfully developed a frequency-stabilized intrinsic fiber-optic Fabry-Perot (FSI-FOFP) sensor for detection of ultrasound [Dorighi, Krishnaswamy & Achenbach (1995b)]. We also have preliminary results on intrinsic and extrinsic laser generation of ultrasound, and we have shown that the signal-to-noise performance of the FSI-FOFP is sufficient to enable the detection of the rather small amplitude ultrasound that is typically generated by laser thermoelastic generation [Dorighi, Krishnaswamy & Achenbach (1994, 1995c,d)]. Applications to the detection of structural flaws and cure monitoring [Dorighi, Krishnaswamy & Achenbach (1995e)] have also been demonstrated with the FSI-FOFP. Another important aspect that we have begun to pursue relates to sensor characterization -- in particular the frequency response of the ultrasonic FOFP sensor [Dorighi, Krishnaswamy & Achenbach (1995a)]. This is essential for correct quantitative interpretation of the acquired data. We have developed analytical FOFP frequency response models by considering the elastodynamic problem of harmonic plane waves propagating normally to the axis of a cylinder (the fiber) embedded in an infinite elastic medium (the bulk structure). We have also done preliminary experiments to simulate the theory and to verify the theoretical predictions.

II. Results from AFOSR Supported Research

2.1 **Sensor Development**: A low finesse intrinsic fiber optic Fabry-Perot (FOFP) sensor was chosen for development as a localized ultrasound sensor [Dorighi, Krishnaswamy & Achenbach (1995b)]. This type of sensor is a localized fiber interferometer which requires the embedding of only one fiber length per sensor, and its intrinsic design does not include any air gaps which are detrimental to the structural integrity of the host [Alcoz (1990)]. Stabilization of this sensor is a key issue which must be addressed before practical applications of this sensor can be realized. The usual method of stretching the fiber sensor region to stabilize a FOFP at its most sensitive point cannot be implemented on embedded FOFPs. We have therefore used the method of tuning the laser frequency to stabilize embedded FOFPs, a technique that was demonstrated by Dandridge et al (1982) for a Mach-Zehnder fiber interferometer. In this section, we show the necessity for the stabilization of embedded FOFPs especially for detecting low amplitude ultrasound in the presence of low frequency but high amplitude dynamic strains.

2.1.1 *Principle of FOFP Sensor:* The fiber optic Fabry-Perot consists of a partially mirrored fiber end face spliced to a small fiber length that has a mirror of approximately the same reflectivity at the other end, as shown in Figure 2.1. As with all interferometers, this sensor produces a change in output intensity which is related to the phase shift of light in the sensing region. Phase shifts are induced by changes in the length and refractive index of the sensing fiber. Consequently, the three dimensional state of strain in the host interacts with the embedded fiber resulting in a change in the intensity reflected from the FOFP.

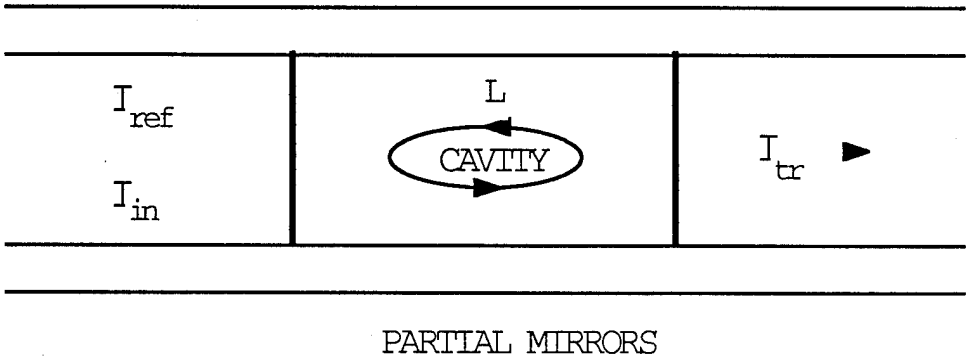

Figure 2.1: Schematic of intrinsic fiber optic Fabry-Perot.

For a Fabry-Perot cavity with low reflectivity mirrors ($R \ll 1$), termed a low finesse Fabry-Perot or a Fizeau interferometer, the reflected intensity is given by:

$$\frac{P_r}{P_i} = 2R(1-\cos\varphi). \qquad (2.1)$$

where: P_r is the intensity of the reflected light, P_i is the intensity of the incident light, R is the reflectivity of the mirrors, and φ is the static phase shift of light in the sensing region. The static phase shift of light in the sensing region is given by:

$$\varphi = \frac{4\pi\nu\ell n}{c} \quad , \qquad (2.2)$$

where: ℓ is the gauge length of the sensor, ν is the frequency of the light, n is the refractive index of the fiber, and c is the speed of light in vacuum. Consequently, the response of a low finesse FOFP is comparable to that of a conventional two beam interferometer.

The reflected intensity from an intrinsic FOFP is plotted in Fig. 2.2 as the light phase in the sensing region is shifted by ramping the laser frequency. We can see that for a large phase shift, the reflected intensity oscillates through many peaks. However, for a small phase shift only local oscillations about a point on this curve will occur. We expect the ultrasound impinging upon a fiber sensor to produce small phase shifts of light, thereby causing the reflected intensity to oscillate about some point on the response curve in Fig. 2.2. This is because typically the displacements associated with ultrasound are small, 1 to 50 nm, compared to the wavelength of the light we are using, 780 nm. When measuring small phase shifts it is clearly desirable to operate along the linear region of the response curve, the region between the peaks and valleys. This is known as operating the sensor at quadrature, when it gives the largest change in reflected intensity for a given phase shift of light. Additionally, at quadrature the relation between small phase shifts and the variation in the reflected intensity is essentially linear.

The intrinsic FOFP must be actively maintained at quadrature due to possible drift of the sensor response resulting from mechanical and thermal induced strains around the embedded sensor. In order to maintain quadrature we have implemented an active homodyne stabilization technique which controls the laser frequency to compensate for sensor drift. The mechanical and thermal drifts are distinguished from the ultrasonic signals of interest by noting that ultrasound frequencies are in a bandwidth from 100 kHz to 10 MHz, which is much higher than the fluctuations due to mechanical strain and temperature, which are typically less than 500 Hz. We therefore track low frequency intensity variations and use a feedback loop with an integral controller to change the laser frequency and bring the interferometer back into quadrature.

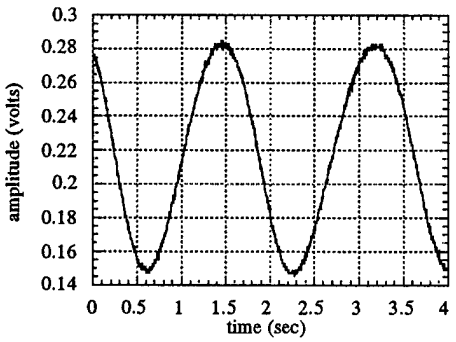

Figure 2.2: Reflected intensity from an intrinsic FOFP as the laser frequency is ramped.

2.1.2 *FOFP Stabilization using Frequency Tuning:* A schematic of the experimental setup to demonstrate the frequency stabilized intrinsic fiber-optic Fabry-Perot (FSI-

FOFP) system is shown in Figure 2.3. Light from an external cavity diode laser (New Focus at 780nm) passes through an optical isolator and is coupled into an ordinary single mode fiber (Corning 4:125). A 2x2 fiber coupler directs a portion of the light toward the fiber sensor with a 10mm gauge length (FiberMetrics) embedded in an epoxy plate (6"x6"x1/2"), the other leg of the coupler is terminated in an index matching gel. The light reflected back from the FOFP is directed toward an avalanche photodiode (APD) which detects both the high frequency intensity variations associated with ultrasound and the low frequency variations due to drift of the sensor. The high frequency signals are high pass filtered and displayed on an oscilloscope, while the low frequency components are used with the stabilization system.

The stabilization loop consists of a differential amplifier which compares the low frequency component of the APD output voltage to a reference voltage representing the quadrature point of the interferometer. The signal from the differential amplifier indicates the amount by which the embedded fiber interferometer is out of quadrature. This signal is input to an op-amp integrator, which determines the frequency response of the stabilization loop, and finally fed back to the laser. The laser frequency is thereby automatically shifted by the amount necessary to bring the fiber interferometer back into quadrature.

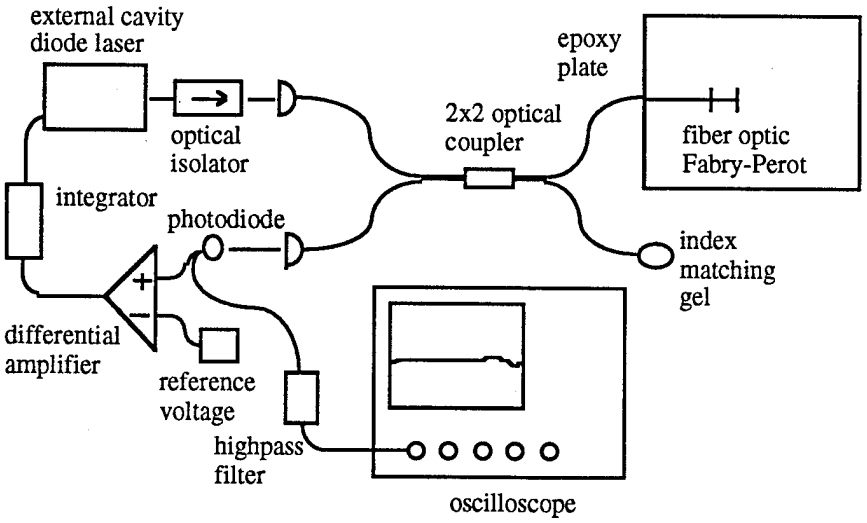

Figure 2.3: Schematic of the setup used for stabilization of the intrinsic FOFP.

To experimentally evaluate the stabilization scheme, we actively induce drift in the fiber sensor by subjecting the structure and the sensor to low frequency dynamic strains. To do this, a vacuum chamber is mounted on one side of the epoxy plate containing the fiber sensor. The vacuum chamber consists of a rubber seal placed between the epoxy specimen and a plexiglas plate. The vacuum chamber input is

regulated using a solenoid valve which cyclically switches between a vacuum reserve and atmospheric pressure. The vacuum is applied for 200 ms before switching to atmospheric pressure for 600 ms to induce low frequency dynamic stressing of the structure and the sensor. The reflected FOFP intensity in the presence of drift induced by low frequency dynamic stressing for the unstabilized and the stabilized sensor are displayed in Figures 2.4a and 2.4b respectively . Without stabilization, the response of the embedded fiber sensor is forced to drift through several fringes, while stabilization maintains the quadrature point.

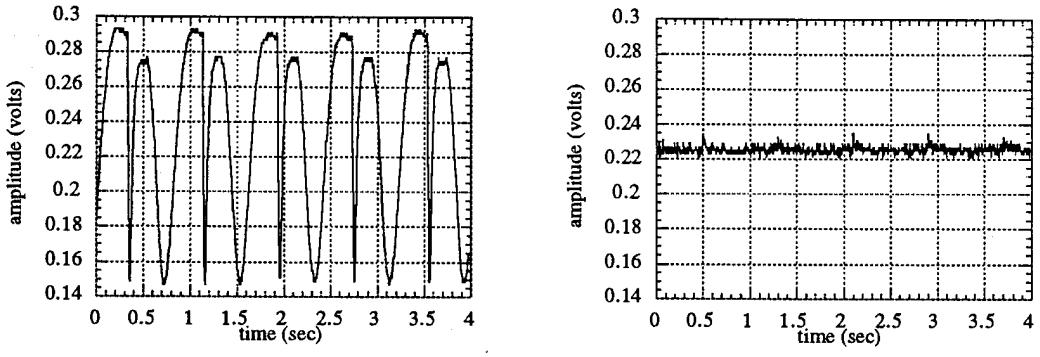

Figure 2.4: Output of (a) an unstabilized and (b) a stabilized FOFP in the presence of induced low frequency drift .

2.2 <u>Sensor Applications:</u> Experiments have been performed to demonstrate that the embedded FOFP can be used for the detection of pzt-transducer and *laser-generated* ultrasound [Dorighi, Krishnaswamy & Achenbach (1995b,c,d)]. In the latter case, elastic waves were generated in the structure using light pulses either incident on the surface of the specimen or coupled into an embedded fiber generator. Applications to flaw detection were also investigated.

2.2.2 *<u>Detection of Piezoelectric Transducer Generated Ultrasound:</u>* [See ref. Dorighi, Krishnaswamy & Achenbach (1995b).] To demonstrate the necessity for sensor stabilization when detecting low amplitude ultrasound, a 5 MHz pulse was generated in the plate using a piezoelectric transducer in the presence of low frequency dynamic strains induced by the vacuum stressing system described in section 2.1.2. The transducer was positioned over the FOFP such that the direction of wave propagation was perpendicular to the embedded sensor. The ultrasonic pulse detected by the unstabilized sensor is displayed in Figure 2.5a, and the corresponding signal with sensor stabilization is shown in Figure 2.5b; both these signals were averaged 30 times. The advantages of

stabilization are obvious when comparing the two figures. In general, the amplitude of the waveforms detected without stabilization in the presence of low frequency strains were not constant in time. This is because when quadrature is not maintained the amplitude of the detected waveform depends on the portion of the response curve over which it is acquired and averaged. This emphasizes that quadrature must be maintained if quantitative comparisons between two waveforms detected by the same sensor are to be made.

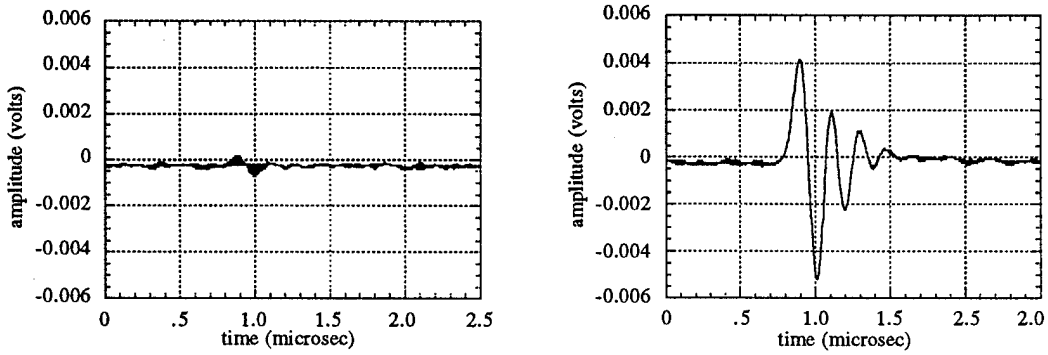

Figure 2.5: Ultrasonic pulse detected using (a) an unstabilized and (b) a stabilized FOFP.

2.2.2 *Detection of Laser Generated Ultrasound:* [See ref. Dorighi, Krishnaswamy & Achenbach (1995c,d)] Ultrasound was also generated using Nd:Yag laser pulses: i) incident on the surface of the plate, and ii) coupled into an embedded fiber generator. A schematic of the two configurations is shown in Figure 2.6. The first configuration (Fig 2.6a) directed a laser pulse with an energy of approximately 12 mJ and a pulse width of 20 ns onto the surface of the epoxy plate. The second configuration used an embedded fiber generator to produce ultrasound (Fig 2.6b). Laser pulses of similar energy and pulse width as those incident on the surface were focused into a high power fiber (3M PowerCore with core diam.=1000μm). The output end of the high power fiber was coated with zinc, spray painted matte black, and embedded in an epoxy plate (3.5"x2.0"x1/2"). Zinc was used for the embedded fiber coating because it possesses a large thermoelastic expansion coefficient. In both of these configurations, the incident laser pulse produced a rapid thermoelastic expansion of the absorbing layer, either zinc or black paint, thereby generating ultrasound in the structure. The surface laser-generated ultrasound (see Fig. 2.6a) and interior laser-generated ultrasonic pulse (Fig 2.6b) were detected by the embedded FOFP and are shown in Figs. 2.7a-b.

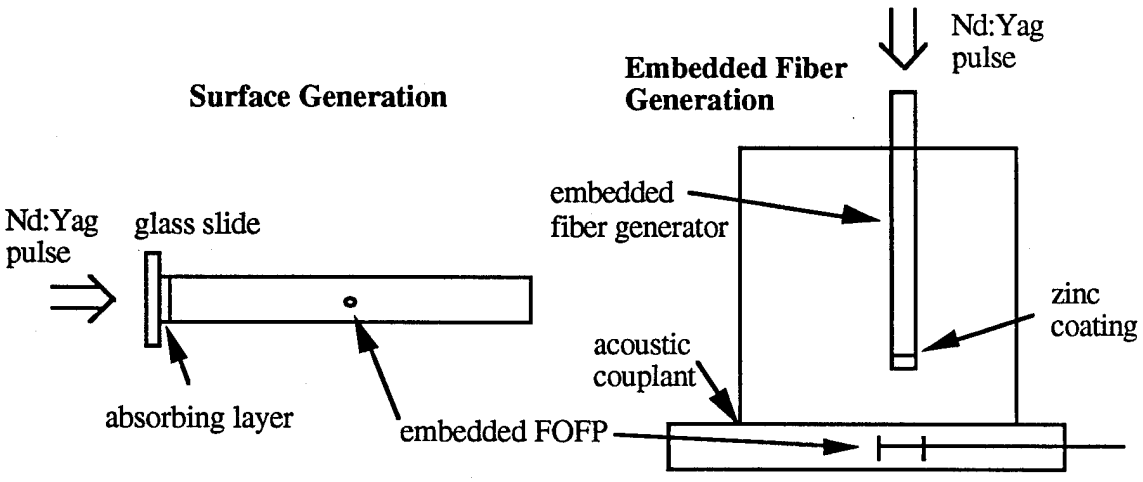

Figure 2.6: Configurations for (a) surface and (b) interior laser generation of ultrasound.

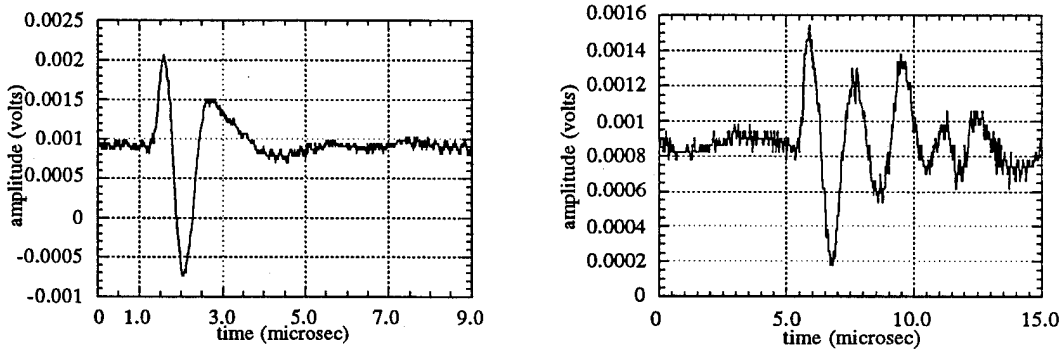

Fig. 2.7:(a) Surface and (b) interior laser-generated ultrasound as detected by FSI-FOFP.

2.2.3 *Applications to Flaw Detection:* The FSI-FOFP sensor was also used to detect the presence of a small hole in an epoxy plate. The schematic of the setup is shown in fig. 2.7a. The pzt-transducer used to generate the ultrasound was 22mm from the sensor and a 3mm diameter hole was drilled 9mm on the other side of the FSI-FOFP sensor. The first pass and reflected signals (if any) from the hole were monitored for various transducer positions. The ratio of the reflected to the incident signal is plotted in fig. 2.7b for different positions of the transducer. The presence of the strong reflected signal for certain transducer positions indicates reflection from the hole.

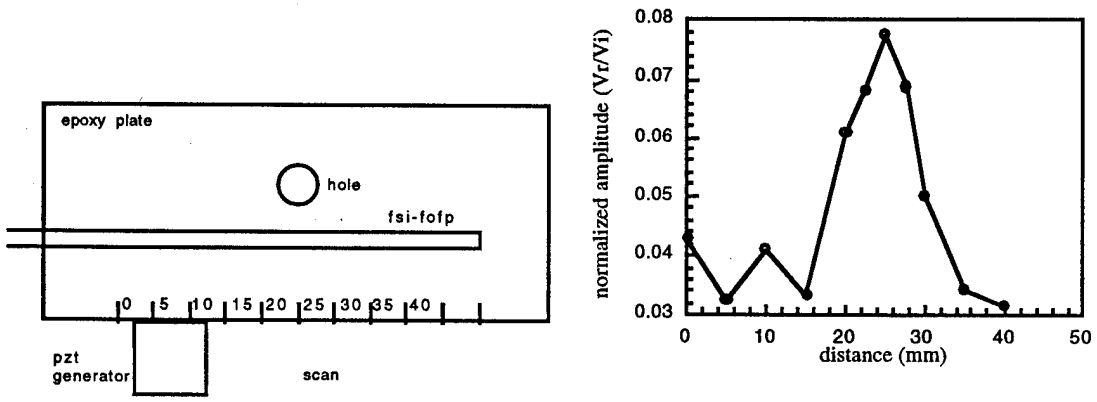

Fig. 2.7: (a) Geometry and (b) defect reflectivity as sensed by the FSI-FOFP sensor.

2.3 Sensor Characterization: [See ref. Dorighi, Krishnaswamy & Achenbach (1995e) and Dorighi (1994)] It is important to determine the frequency response of the fiber sensors in order to establish the ultrasonic frequencies over which such sensors will be suitable. A theoretical basis can be laid for calculating the frequency response assuming a simplified sensor geometry. The geometry considered is displayed in Figure 2.8. The intrinsic fiber-optic Fabry-Perot is modeled as an infinitely long cylindrical elastic inclusion embedded in a host. Both the host and the inclusion are assumed to be linearly elastic, isotropic, and homogeneous but with differing material properties. Consequently, we are neglecting differences in the material properties between the fiber core and cladding. A harmonic plane wave impinges upon the x_2-axis of the cylinder, producing scattered and refracted waves at the interface. Plane strain conditions such that no displacements occur along the x_1-axis are assumed to hold.

The incident elastic wave strain can be related to the phase shift of light in the sensing region through the following steps: i) relate incident elastic wave strain to the strain in the fiber core due to the refracted wave following Flax (1982), ii) relate the fiber core strain to changes in the refractive index of the sensing region following Sirkis (1993), and iii) relate refractive index changes to the phase shift of light in the sensing region.

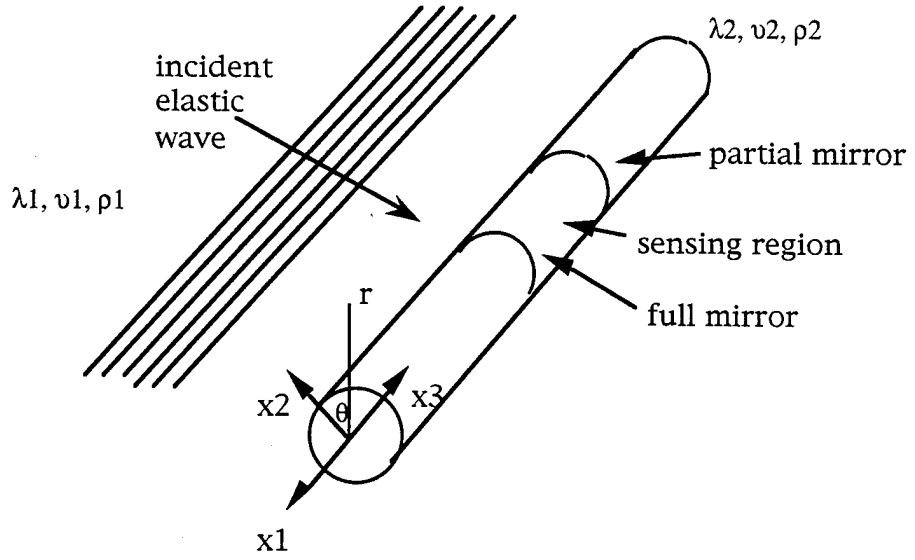

Figure 2.8: Geometry for analysis

2.3.1 *Determination of Strain in the Fiber Core:* In order to determine the refracted wave strain inside the scatterer (fiber) we begin with the displacement equation of motion in an elastic solid given as [Achenbach (1973)]:

$$\mu\nabla^2\underline{\mathbf{u}} + (\lambda+\mu)\nabla\nabla\bullet\underline{\mathbf{u}} = \rho\ddot{\underline{\mathbf{u}}} \tag{2.3}$$

where: μ and λ are the Lame elastic constants, ρ is the density, and $\underline{\mathbf{u}}$ is the displacement vector. The displacement vector can be decomposed into a scalar and vector potential of the form:

$$\underline{\mathbf{u}} = \nabla\phi + \nabla\times\underline{\psi} \tag{2.4}$$

where: ϕ is the scalar potential, and $\underline{\psi}$ is the vector potential. If this expression is substituted into the equation of motion we obtain the following scalar and vector wave equations:

$$\nabla^2\phi = \frac{1}{c_L^2}\ddot{\phi} \quad \text{and} \quad \nabla^2\underline{\psi} = \frac{1}{c_T^2}\ddot{\underline{\psi}} \tag{2.5}$$

where c_L and c_T are respectively the longitudinal and transverse wave speeds in the solid. Recall that we are considering the case of plane strain, so that the only nonzero vector potential is $\psi_1(r,\theta,t)$. This allows us to write $\underline{\psi}(r,\theta,t) = \psi_1(r,\theta,t)\underline{e_1}$, and to further simplify our notation we will express $\psi_1(r,\theta,t)$ as $\psi(r,\theta,t)$. The time

dependence can be eliminated because we are considering the special case of harmonic waves. Thus:

$$\phi(r,\theta,t) = \phi(r,\theta)e^{-i\omega t} \quad \text{and} \quad \psi(r,\theta,t) = \psi(r,\theta)e^{-i\omega t} \tag{2.6}$$

where ω is the frequency of the elastic wave. Substituting these expressions into equations (2.5) we can solve for $\phi(r,\theta)$ and $\psi(r,\theta)$ using separation of variables in cylindrical coordinates. The solutions to these equations allow us to express ϕ and Ψ as infinite series in terms of Bessel Functions and sines or cosines. We now must define specific forms for the incident, scattered, and refracted wave potentials.

The incident harmonic wave is a longitudinal plane wave and can be represented in terms of a scalar potential as follows:

$$\phi^{in} = P_o e^{i\alpha_1 x_2} e^{-i\omega t} = P_o e^{i\alpha_1 r\cos\theta} e^{-i\omega t} = P_o \sum_{n=0}^{\infty} e_n i^n J_n(\alpha_1 r)\cos(n\theta)e^{-i\omega t} \tag{2.7}$$

where P_O is the magnitude of the incident scalar wave, α_1 is the longitudinal wave number in the host, e_n is the Neumann factor (e_O=1, e_n=2 n>0), i is a pure imaginary number, and J_n represents the Bessel function of order n. We require the scattered field to vanish far from the origin, which gives the scattered wave potentials in the following form:

$$\phi^{scatt} = \sum_{n=0}^{\infty} A_n H_n^1(\alpha_1 r)\cos(n\theta)e^{-i\omega t} \quad \text{and} \quad \psi^{scatt} = \sum_{n=0}^{\infty} B_n H_n^1(\beta_1 r)\sin(n\theta)e^{-i\omega t} \tag{2.8}$$

where: A_n and B_n are the magnitude of the scattered fields, β_1 is the transverse wave number in the host medium and H_n^1 are Hankel functions of the first kind of order n. The refracted field must remain finite at the origin which requires that the potentials have the form:

$$\phi^{refr} = \sum_{n=0}^{\infty} C_n J_n(\alpha_2 r)\cos(n\theta)e^{-i\omega t} \quad \text{and} \quad \psi^{refr} = \sum_{n=0}^{\infty} D_n J_n(\beta_2 r)\sin(n\theta)e^{-i\omega t} \tag{2.9}$$

where: C_n and D_n are the magnitudes of the refracted potentials, α_2 and β_2 are respectively the longitudinal and shear wave numbers in the scatterer. In order to solve for the unknown coefficients A_n, B_n, C_n, and D_n we must insist on displacement and traction continuity at the fiber/host interface:

$$\tau_{rr}^{in} + \tau_{rr}^{scatt} = \tau_{rr}^{refr} \tag{2.10}$$
$$\tau_{r\theta}^{in} + \tau_{r\theta}^{scatt} = \tau_{r\theta}^{refr} \tag{2.11}$$
$$u_r^{in} + u_r^{scatt} = u_r^{refr} \tag{2.12}$$
$$u_\theta^{in} + u_\theta^{scatt} = u_\theta^{refr} \tag{2.13}$$

where: u_r and u_θ are the radial and transverse components of displacement, τ_{rr} is the normal stress in the r-direction, and $\tau_{r\theta}$ is the shear stress. The above gives four sets of equations for the four sets of unknowns A_n, B_n, C_n, and D_n. Solving for these unknowns allows the strain in the fiber to be calculated as:

$$\varepsilon_{rr} = \sum_{n=0}^{\infty}\left\{C_n\alpha_2^2 J_n''(\alpha_2 r) - D_n\left[\frac{n}{r^2}J_n(\beta_2 r) + \frac{n\beta_2}{r}J_n'(\beta_2 r)\right]\right\}\cos(n\theta) \tag{2.14}$$

$$\varepsilon_{\theta\theta} = \sum_{n=0}^{\infty}\left\{C_n\left[-\frac{n^2}{r^2}J_n(\alpha_2 r) + \frac{\alpha_2}{r}J_n'(\alpha_2 r)\right] + D_n\left[\frac{n}{r^2}J_n(\beta_2 r) - \frac{n\beta_2}{r}J_n'(\beta_2 r)\right]\right\}\cos(n\theta) \tag{2.15}$$

$$\varepsilon_{r\theta} = \frac{1}{2}\sum_{n=0}^{\infty}\left\{C_n\left[\frac{2n}{r^2}J_n(\alpha_2 r) - \frac{2\alpha_2 n}{r}J_n'(\alpha_2 r)\right] - D_n\left[\frac{n^2}{r^2}J_n(\beta_2 r) + \frac{\beta_2}{r}J_n'(\beta_2 r) + \beta_2^2 J_n''(\beta_2 r)\right]\right\}\sin(n\theta). \tag{2.16}$$

Notice the shear strain given by equation (2.16) vanishes at $\theta = 0$ degrees. This indicates the directions parallel and perpendicular to the incident wave propagation direction are principal strain axes. Ultimately, we are interested in determining the strain field along the principal strain axes in the fiber core (i.e. at r=0), where the light is propagating. This strain field is given by the radial component of strain at $\theta = 0$ and $\theta = 90$ degrees. The radial strain in the fiber core can be rewritten as:

$$\varepsilon_{rr} = \sum_{n=0}^{\infty}\left\{C_n\left[\alpha_2^2 J_{n-2}(\alpha_2 r) - \frac{\alpha_2(2n-1)}{r}J_{n-1}(\alpha_2 r) + \frac{(n^2+n)}{r^2}J_n(\alpha_2 r)\right] + D_n\left[\frac{\beta_2 n}{r}J_{n-1}(\beta_2 r) - \frac{(n^2+n)}{r^2}J_n(\beta_2 r)\right]\right\}\cos(n\theta). \tag{2.17}$$

An important simplification occurs if we note that the diameter of the fiber core is small compared to diameter of the fiber cladding, 4 μm compared to 125 μm. This allows us to use the following approximation for the Bessel function as r -> 0 [Hildebrand (1976)]:

$$J_n(r) \approx \frac{1}{2^n n!} r^n. \tag{2.18}$$

Substituting this into equation (2.17) we have for the radial strain in the fiber core

$$\varepsilon_{rr} \approx C_o \frac{\alpha_2^2}{2} + \left[-C_2 \frac{\alpha_2^2}{4} + D_2 \frac{\beta_2^2}{4} \right] \cos(2\theta). \tag{2.19}$$

Consequently, it is only necessary to solve for three coefficients C_0, C_2, and D_2 to determine the strain in the fiber core. Note also that the strain in the fiber core varies as a function of θ, which indicates that different polarizations of light will undergo different phase shifts in the sensing region.

2.3.2 *Relation between the Strain in the Fiber Core and the Phase Shift of Light:* The total phase shift of light in the sensing region of the fiber is given as:

$$\varphi_2^{tot} = \varphi_2 + \Delta\varphi_2 l \qquad \text{and} \qquad \varphi_3^{tot} = \varphi_3 + \Delta\varphi_3 l \tag{2.20}$$

where: φ_2^{tot} and φ_3^{tot} are the total phase shifts along the two principal strain axes, φ_2 and φ_3 are the static phase shifts, $\Delta\varphi_2$ and $\Delta\varphi_3$ are strain and temperature induced phase shifts per unit length, and l is the length of the sensing region. Neglecting temperature induced phase shifts, we can represent the phase shift of light along the two principal strain axes due to impinging ultrasound as [DePaula (1982), Sirkis (1993)]:

$$\Delta\varphi_2 = -kn_o^3 \left[P_{11}\varepsilon_{rr}^{\theta=0} + P_{12}\varepsilon_{rr}^{\theta=90} \right] \qquad \text{and} \qquad \Delta\varphi_3 = -kn_o^3 \left[P_{11}\varepsilon_{rr}^{\theta=90} + P_{12}\varepsilon_{rr}^{\theta=0} \right] \tag{2.21}$$

where: k is the wave number of the light, n_o is the static refractive index of the fiber core, P_{11} and P_{12} are the Pockels strain-optic coefficients. Equations (2.20-21) assume the acoustically induced strains are small enough to only act as a perturbation to the refractive index of the fiber. Note also that the phase shift of light is only a function of changes in the refractive index because we have assumed the case of plane strain. In

general, strain along the axis of the fiber will also contribute to phase changes of light in the sensing region.

2.3.3 *Frequency Response of Embedded and Submerged Fiber Sensors:* We have calculated the phase shift of light in a fiber sensor as a function of the incident ultrasonic frequency using the outlined approach. Two different situations were considered: a fiber situated in water, and a fiber embedded in epoxy. For the case of a fiber in water, we only have to consider scalar potentials in the host medium because water treated as inviscid is not able to support shear waves. This simplifies the analysis in that the shear traction continuity condition is not needed. It also allows us to compare our calculations with published results. However, when determining the frequency response of an embedded fiber, it is necessary to use the complete analysis.

Experiments to verify the above analytical models were also conducted. For simplicity, we used a long cavity frequency-stabilized fiber-optic Fabry-Perot sensor consisting of a polarization maintaining lead-in fiber segment spliced to a short segment of ordinary single-mode (SM) fiber as shown in fig. 2.9. The PM fiber segment is necessary to minimize polarization fading and to launch light in either of two orthogonally-polarized modes into the sensor. However, since PM fibers have stressing elements that can distort the impinging ultrasound, the insonification region was only over the ordinary SM fiber segment. For the case of fiber situated in water, the bare fiber sensor was held in a water tank with an immersion pzt-transducer as shown in fig. 2.9. For the case of the fiber sensor embedded in epoxy, the entire epoxy plate containing the fiber was immersed in the water tank. A 5MHz pzt-generator was frequency swept over its bandwidth, and the ultrasound was monitored with the fiber sensor for light launched into both polarization modes. The resulting signal was deconvolved to account for all but the fiber-sensor response as explained in Dorighi (1994). Figures 2.10 and 2.11 show the theoretically expected and the experimentally determined response for the cases of the FOFP in water and the FOFP embedded in epoxy respectively. An interesting point to note is that the FOFP embedded in epoxy is actually a very broadband ultrasound transducer with essentially a flat response.

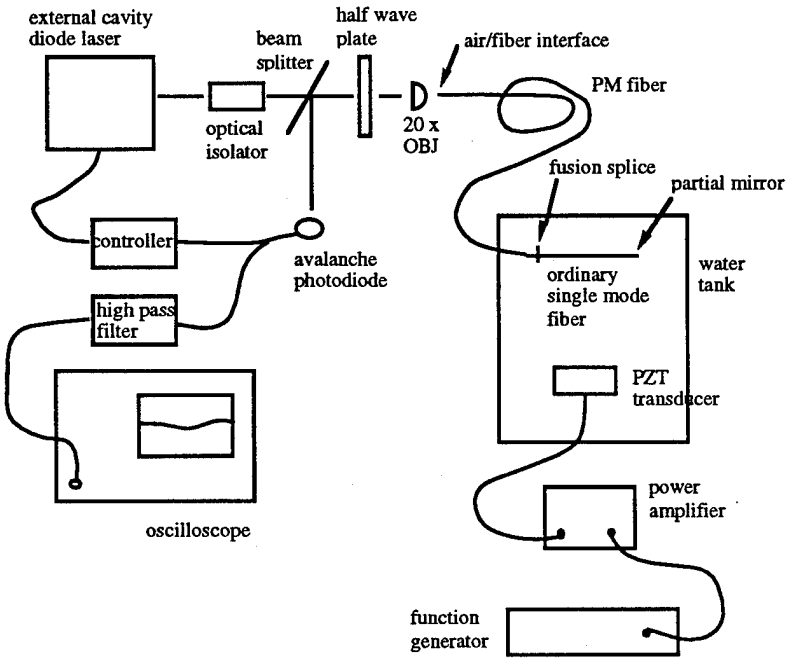

Fig. 2.9: Experimental setup to measure the frequency response of the FOFP

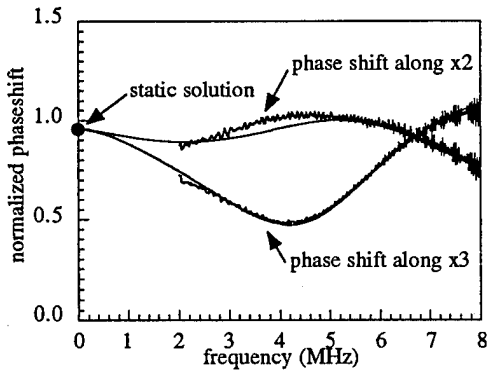

Fig. 2.10: Theoretical and measured frequency response for bare fiber sensor in water

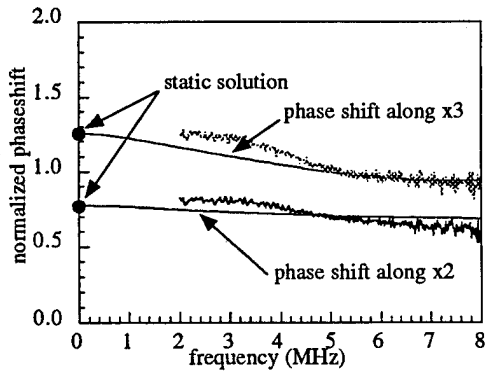

Fig. 2.11: Theoretical and measured frequency response for fiber sensor in epoxy

III. Conclusions

Critical issues pertaining to the development of a fiber optic ultrasound system for use in a 'smart structure' have been addressed. The primary issues which have been investigated in this work are: i) the stabilization of a localized fiber optic interferometer at its quadrature point for the detection of ultrasound, ii) the development of a fiber optic scheme for the generation of ultrasound, iii) the development of a theoretical model which predicts the frequency response of an embedded fiber ultrasound sensor for a given host materials, and iv) an experimental verification of the theoretical model.

The localized fiber optic Fabry-Perot interferometer was stabilized at its quadrature point by tuning the frequency of the laser source to compensate for thermal and mechanical drifts. This technique eliminates the need for a piezoelectric fiber stretcher and allows the fiber sensor to be embedded at any desired location inside a structure. The utility of this scheme was demonstrated by inducing mechanical strains in a plate containing an embedded fiber sensor and actively stabilizing the interferometer by tuning the laser frequency. Furthermore, ultrasound was detected by the stabilized fiber sensor in the presence of mechanical strains.

A fiber optic technique for the generation of ultrasound has been developed. Using a high power laser source and an optical fiber for the generation of ultrasound creates a system which is resistant to corrosion, has the ability to operate at high temperatures, and can generate ultrasound at a location of interest within a structure. One of the techniques developed uses an optical fiber which is embedded in the structure of interest, while the second technique generates ultrasound at the surface of a specimen. Both of these schemes complement the advantages of fiber optic ultrasound sensors.

Finally, a theoretical model was developed which predicts the response of an embedded fiber interferometer. Calculations were performed for a fiber submerged in water and embedded in epoxy. Both of these configurations were experimentally verified. This is an important development because now that a model has been developed and confirmed, the response of a fiber optic sensor embedded in a host with different material properties can be predicted simply by using the model.

IV. References

Achenbach, J.D., (1973), Wave Propagation in Elastic Solids, American Elsevier.

Agrawal G.P., (1995), "Nonlinear Fiber Optics," Academic Press.

Alcoz J. et al, (1990), *Embedded Fiber-Optic Fabry-Perot Ultrasound Sensor*, IEEE Trans. Ultrasonics, Ferroelectrics, and Frequency Control, Vol. 37, No. 4.

Claus R.O. and C.D. Thompson, (1991), *Optical Fiber-Based Ultrasonic Wave Generation and Detection in Materials,* Review of Progress in Quantitative Nondestructive Evaluation, vol. 10B, Plenum press, New York.

Cole JH., R.L. Johnson and P.G. Bhuta, (1977), in J. Acoust. Soc. Am., vol. 62, No. 5.

Dandridge A. et al, (1982),*Homodyne Demodulation Scheme for Fiber Optic Sensors using Phase Generated Carrier*, IEEE J. Quantum Electronics, Vol. QE-18, No. 10.

Davis M.A. , A.D. Kersey, J.S. Sirkis, and E.J. Frieble, (1994), "Fiber optic Bragg grating array for shape and vibration mode sensing," in SPIE Proc. vol. 2191.

DePaula, R.P. et al, (1982),*Single-Mode Fiber Ultrasonic Sensor*, IEEE Journal of Quantum Electronics, Vol. QE-18, No. 4.

Dorighi, J.F., Sridhar Krishnaswamy and Jan D. Achenbach, (1994), "Embedded Fiber-Optic Fabry-Perot Sensors for Ultrasound Detection," in Rev. Progress in QNDE, ed. D.O. Thompson and D.E. Chimenti, vol. 14, Plenum Press, New York.

Dorighi, J.F., Sridhar Krishnaswamy and Jan D. Achenbach, (1995a), "Frequency Response of Fiber Optic Ultrasound Sensors," to appear Proc. IEEE UFFC Symposium, Seattle, Nov. 7-10, 1995.

Dorighi, J.F., Sridhar Krishnaswamy and Jan D. Achenbach, (1995b), "Stabilization of an Embedded Fiber-Optic Fabry-Perot Sensor for Ultrasound Detection," IEEE Transactions on Ultrasonics, Ferroelectrics and Frequency Control, vol .42, No. 5.

Dorighi, J.F., Sridhar Krishnaswamy and Jan D. Achenbach, (1995c), "Fiber-Optic Laser Generation and Detection of Ultrasound", SPIE Proceedings, vol 2574, pp.46-53.

Dorighi, J.F., Sridhar Krishnaswamy and Jan D. Achenbach, (1995d), "Laser-based Ultrasonics using Fiber-Optic Laser Generation and Detection of Ultrasound", to appear in the Proceedings of the Optical Engineering Midwest, Chicago, May 18-20, 1995.

Dorighi, J.F., Sridhar Krishnaswamy and Jan D. Achenbach, (1995e), "Stabilization of an Embedded Fiber-Optic Ultrasound Sensor for Cure Monitoring of an Epoxy Plate," in Rev. Progress in QNDE, ed. D.O. Thompson and D.E. Chimenti, vol. 15, Plenum Press.

Dorighi, J.F., (1994), M.S. Dissertation, Northwestern University.

Dunphy J.R., G. Metz, and W. Morey, (1995), "Optical Fiber Bragg Grating Sensors," in Fiber Optic Smart Structures, ed. Eric Udd, Wiley.

Flax L., V.K. Varadan and V.V. Varadan, (1980), "Scattering of an obliquely incident acoustic wave by an infinite cylinder," J. Acoust. Am, vol. 68, No. 6.

Flax L., et al, (1982), *Acoustically Induced Birefringence in Optical Fibers*, Journal of the Optical Society of America, Vol 72, No. 9,

Grattan KTV,& B.T. Meggitt, (1995), "Optical Fiber Sensing Technology," Chapman UK

Hildebrand, F.B., (1976), Advanced Calculus for Applications, Prentice-Hall, New Jersey

Huang S., M. LeBlanc, M.M. Ohn and R.M. Measures, (1995), Appl. Opt., vol. 34 (22).

Kersey A.D. (1992), SPIE Proceedings vol. 1797.

Measures, R.M., (1991), in Rev. Prog. QNDE, vol. 10B, Plenum press, New York.

Morey W.W, (1995), "Fiber optic grating technology," in SPIE Proc. vol. 2574.

Narendran N, S. Letcher, A. Shukla, and R. Singh, (1992), in SPIE Proc. vol. 1798.

Sirkis J. (1993), Optical Engineering, vol. 32, No.4.

Udd, E. (1995), "Fiber Optic Smart Structures," John Wiley, New York.

Udd E., (1991), Fiber Optic Sensors: An Introduction for Engineers and Scientists," John Wiley, New York.